New Phytologist

Research

Antisense reduction in NADP-ME in the C_4 species *Flaveria bidentis* alters stomatal sensitivity to intercellular [CO_2]

Emmanuel L. Bernardo[1,2], Cristina Rodrigues Gabriel Sales[1], Tianshu Sun[1] and Johannes Kromdijk[1]

[1]Department of Plant Sciences, University of Cambridge, Downing Street, CB23EA, Cambridge, UK; [2]Institute of Crop Science, University of the Philippines Los Baños, College of Agriculture and Food Science, Los Baños, 4031, Laguna, Philippines

Author for correspondence:
Johannes Kromdijk
Email: jk417@cam.ac.uk

Received: *27 June 2025*
Accepted: *26 January 2026*

New Phytologist (2026)
doi: 10.1111/nph.71012

Key words: C_4 photosynthesis, CO_2 assimilation, *Flaveria bidentis*, NADP-ME, photosynthesis, stomatal conductance.

Summary

- Stomata have the crucial role of balancing the uptake of CO_2 for photosynthesis and water loss via transpiration by adjusting their aperture. In C_3 plants, coordination between photosynthesis and stomatal conductance can be disrupted by mutations in Calvin–Benson–Bassham (CBB) cycle expression, but it is not clear whether the disruption of the C_4 carbon concentrating mechanism would have similar effects.
- In this study, it was hypothesized that perturbing the C_4 cycle, resulting in reduced carbon flux into the bundle sheath cells and overall net CO_2 assimilation rates, may alter stomatal regulation. To test this hypothesis, we performed gas exchange measurements on transgenic *Flaveria bidentis* plants carrying an antisense construct leading to reduced nicotinamide adenine dinucleotide phosphate (NADP)-malic enzyme (NADP-ME) activity.
- Stomatal conductance was unaltered in the antisense plants at ambient CO_2 levels. However, C_i was significantly increased. When measurements were instead performed at common C_i, stomatal conductance was significantly higher in the antisense lines.
- These results demonstrate that disruption of the C_4 cycle via reduced NADP-ME activity in *F. bidentis* leads to altered stomatal sensitivity to C_i.

Introduction

Stomatal pores on the leaf epidermis regulate gas exchange between plants and the atmosphere. By adjusting their aperture through guard cell turgor changes, stomata balance CO_2 uptake for photosynthesis with water loss via transpiration. Plants must therefore continuously optimize stomatal aperture to maximize CO_2 uptake while minimizing dehydration, which is achieved through dynamic responses to environmental and internal signals. In general, stomata open when conditions favor carbon assimilation and close under stress or excess CO_2. For instance, stomatal apertures widen when exposed to low CO_2 concentrations, high light, and high humidity but close under high CO_2, darkness, low humidity, high temperature, and drought (Farquhar & Sharkey, 1982; Marshall *et al.*, 1996; Fricker & Willmer, 2012). By making these coordinated adjustments, plants maintain efficient gas exchange and water balance essential for survival in changing environments.

One key regulator of stomatal opening and closing is the concentration of CO_2 inside the leaf (intercellular CO_2, C_i). Guard cells are thought to respond to changes in C_i rather than CO_2 (C_a), forming a feedback loop between photosynthesis and stomatal conductance (Mott, 1988, 2009). An increase in C_i (as during the night or in CO_2-rich air) triggers guard cells to lose turgor and close, whereas a decrease in C_i (as during photosynthesis) induces stomatal opening. Although this mechanism is often described as guard cell autonomous, as shown by the fact that responses are maintained in epidermal peel experiments that lack mesophyll tissue (Fitzsimons & Weyers, 1986), subsequent studies indicate that mesophyll-derived signals are required for complete stomatal responses to CO_2 (Engineer *et al.*, 2016).

Mesophyll cells can modulate stomatal behavior by producing diffusible metabolites, which can accumulate in the apoplast surrounding guard cells and relay information about the leaf's photosynthetic activity (Engineer *et al.*, 2016; Taylor *et al.*, 2025). For example, red light often induces stomatal opening even when C_i is held constant, demonstrating a C_i-independent response that likely involves photoreceptor or mesophyll-derived signals (Messinger *et al.*, 2006; Taylor *et al.*, 2024). Thus, additional links between mesophyll photosynthesis and guard cell autonomous sensing pathways are apparent (Lawson *et al.*, 2014), and guard cells do not only adjust to C_i but also integrate additional mesophyll-derived signals or light-dependent cues, collectively termed C_i-independent responses, to fine-tune stomatal aperture. Meanwhile, C_i-dependent responses are those directly controlled by changes in intercellular CO_2 concentration sensed by guard cells (Messinger *et al.*, 2006; Lawson *et al.*, 2008).

While coordination between stomatal conductance and photosynthetic rate is typically tight, they can be decoupled through transgenic manipulations. Previous studies in transgenic plants demonstrated that antisense reduction in Calvin–Benson–

© 2026 The Author(s).
New Phytologist © 2026 New Phytologist Foundation.
This is an open access article under the terms of the Creative Commons Attribution License, which permits use, distribution and reproduction in any medium, provided the original work is properly cited.

Bassham (CBB) cycle enzyme activities such as Rubisco (Furbank *et al.*, 1996), phosphoribulokinase (Paul *et al.*, 1995), glyceraldehyde-3-phosphate dehydrogenase (Price *et al.*, 1995), or chloroplastic fructose-1,6-bisphosphatase (Muschak *et al.*, 1999) can severely decrease photosynthetic capacity but with little or no change in stomatal conductance. For instance, tobacco plants with < 25% of normal Rubisco content maintained near-normal g_s under high light (von Caemmerer *et al.*, 2004). Across many of these studies, antisense plants exhibited elevated C_i levels without stomatal closure. However, while many of these studies reported observations of g_s, the experiments were generally not designed to wait long enough for the stomatal responses to fully unfold nor account for indirect physiological effects on g_s such as increases in C_i when A decreases, which complicate the interpretation of stomatal responses in these studies (Lawson, 2009). Indeed, when SBPase antisense plants were compared under controlled C_a, as is most common, g_s was found to be different, but so was C_i (Lawson *et al.*, 2008). However, when g_s was measured under common C_i, differences were no longer apparent. This demonstrates the importance of assessing the impact of such confounding effects. Furthermore, the degree to which the stomata open or close (and therefore g_s changes) depends on the stomatal anatomical and morphological characteristics, including stomatal density (SD, the number of stomata per leaf area), which can be further affected by the prevailing growth conditions (Casson & Gray, 2008; Torii, 2015) and may also be perturbed by antisense manipulations of CO_2 fixation. Nevertheless, only a few studies investigating the impact of antisense reduction of A_n on stomatal conductance account for potential confounding effects of both C_i and stomatal patterning.

C_4 plants provide an attractive experimental setup to evaluate the impact of antisense reduction in A_n on stomatal conductance for several reasons. First, because of the presence of the C_4 carbon concentrating mechanism, A_n is typically (close to) CO_2-saturated in C_4 plants (Pignon & Long, 2020). As a result, changes in g_s in response to experimentally varying C_a or C_i can be interpreted without the confounding effect of simultaneous impacts on A_n. Second, adjusting the carbon uptake flux by perturbing C_4 cycle activity should not directly affect guard cell photosynthesis, in contrast to many Calvin cycle mutants. Because of these reasons, mutants in C_4 cycle enzymes avoid some of the common caveats to verify whether changes in mesophyll carbon flux modify stomatal behavior through C_i-dependent or C_i-independent mechanisms.

Here, we investigated stomatal regulation in transgenic C_4 *Flaveria bidentis* plants with reduced nicotinamide adenine dinucleotide phosphate (NADP)-malic enzyme (NADP-ME) activity. In C_4 plants, NADP-ME is the key decarboxylase in the C_4 cycle that converts malate to pyruvate leading to the release of CO_2 in the chloroplasts of bundle sheath cells. Reducing NADP-ME activity limits malate decarboxylation and delivery of nicotinamide adenine dinucleotide phosphate (NADPH) and CO_2. We hypothesized that this perturbation of the C_4 cycle would alter the coordination between CO_2 assimilation and stomatal conductance by affecting either the C_i signal perceived by the guard cells or via C_i-independent signals linked to mesophyll carbon metabolism. While responses to red light and stomatal sensitivity to blue light were unaffected by the decrease in NADP-ME activity, NADP-ME antisense lines of *Flaveria bidentis* had higher operational C_i at ambient CO_2 levels than wild-type (WT). When additional measurements were performed under common C_i, g_s was significantly increased in the antisense lines. These findings imply that stomatal movements in these plants are adjusted to maintain transpiration via altered stomatal sensitivity to C_i. In addition, the lack of differences at ambient CO_2 levels may suggest that the CO_2 levels sensed by guard cells may include a contribution of C_a.

Materials and Methods

Plant materials

WT and T_1 seeds of NADP-ME antisense *Flaveria bidentis* (L.) were provided by Prof. Susanne von Caemmerer (Australian National University, Canberra, Australia). The antisense construct used to generate the transgenic lines was originally described by Pengelly *et al.* (2010) and consisted of an 845-bp fragment in antisense orientation from the central coding region of ChlME1, the primary chloroplastic C_4 isoform of NADP-ME identified in *F. trinervia* and *F. bidentis* (GenBank accession nos. X57142 and AY863144). The T-DNA cassette contained the CaMV 35S promoter, the NADP-ME antisense fragment, a Nos terminator, and a kanamycin resistance cassette for selection. Seven independent transformation events were generated, coded as 1A-4, 1A-5, 1A-6, 1A-7, 1A-8, 2A-1, and 2A-2. Two out of three specific antisense events used in this study (1A-5, 1A-8, and 2A-1) were independent from those previously characterized in Pengelly *et al.* (2012) and represent additional transgenic events derived from the same construct.

PCR confirmation and copy number estimation

The presence of the NeoR/KanR selectable marker gene was confirmed via PCR using primers AATGAACTGCAGGAC GAGGC and AATGAACTGCAGGACGAGGC. Copy number analysis was performed following Głowacka *et al.* (2016) using reverse transcription polymerase chain reaction (RT-PCR) on genomic DNA with FbACTIN gene as a reference amplicon (AATGGAAGCTGCTGGTATTCA) and (CAACCACCTTG ATCTTCATGC primers).

Growth conditions

WT and T_1 seeds were sown in plastic pots (10 cm H × 9 cm L × 9 cm W) filled with M3 compost (Levington®; Scotts, Ipswich, UK). The substrate was amended with controlled-release fertilizer (Osmocote®; Scotts Miracle-Gro Company, Marysville, OH, USA) at a rate of 1.0–1.5 g l^{-1} substrate. Plants were grown in controlled-environment chambers (Conviron®; Controlled Environments Ltd, Winnipeg, MB, Canada) in a 12 h : 12 h, day : night cycle at 20°C, 65% RH, and a photon flux density (PFD) of 350 µmol m^{-2} s^{-1}. The

© 2026 The Author(s).
New Phytologist © 2026 New Phytologist Foundation.

plants were hand-watered to field capacity twice a week. PCR-confirmed T_1 plants carrying a single copy integration of the NADP-ME antisense construct were self-pollinated to obtain T_2 seeds. T_2 homozygous plants were grown under similar conditions as the T_1 generation, but with a lower PFD of 150 μmol m^{-2} s^{-1}, since plants exposed to 350 μmol m^{-2} s^{-1} showed leaf bleaching (Supporting Information Fig. S1) in the antisense plants. These growth conditions resulted in mutant plants, which looked identical to WT plants and grew at similar rates (Fig. S2). T_2 plants were self-pollinated, and the seeds were collected to generate T_3 homozygous lines. All phenotyping was performed on 8-wk-old plants from T_3 homozygous lines using the second or third recently expanded leaf.

Protein and Chl content

Three replicate disks with a total area of 1.5 cm^2 were collected using metal cork borers from recently expanded leaves from the same plants measured for gas exchange. Samples were flash-frozen in liquid N_2 and then stored at −80°C for further use. Frozen leaf samples (1.5 cm^2) were homogenized in ice-cold mortar and pestle into basic extraction buffer. Chls were extracted from 40 μl crude leaf extract in 960 μl 80% ethanol. The solution was incubated at 22°C (room temperature) in the dark for 2 h, and the absorbance was determined spectrophotometrically at 649 and 665 nm, allowing calculation of Chl content following Wintermans & De Mots (1965). Protein content was estimated against Bovine Serum Albumin (BSA) standards using Bradford assay (Sigma, Product No. B6916).

SDS-PAGE and immunoblot analysis

SDS-PAGE was performed using 2 μg of total protein from each sample. Blotting of proteins to polyvinylidene difluoride (PVDF) membranes was performed using *Trans*-Blot Turbo RTA Transfer Kit, PVDF (BIO-RAD Laboratories Inc.) according to the manufacturer's instructions. Before assembly, the PVDF membrane was briefly activated with absolute methanol. Both the PVDF membrane and the filter paper were then soaked and equilibrated in 1× transfer buffer (diluted from the stock solution of Trans-Blot Turbo 5× transfer buffer, BIO-RAD Laboratories Inc. (Cat. No. 10026938)). Transblotting of western blot sandwich was performed using the Trans-Blot Turbo Transfer System (BIO-RAD Laboratories Inc., Hercules, CA, USA). All subsequent steps were performed on the blotted membranes under gentle agitation (60–100 rpm) using a horizontal shaker (Ultimax 1010; Heidolph Instruments, Schwabach, Germany). Membranes were first immersed in 1× Tris buffered saline (TBS) buffer (88 mM Tris base, 2.5 M NaCl, and adjusted to pH 7.5 with HCl) with sufficient volume covering the membrane. After washing, the membrane was blocked with 5% (w/v) nonfat milk in Tween-TBS (TTBS) buffer (1× TBS, 0.05% (v/v) Tween-20) for 60 min at room temperature. The membranes were then washed twice with TTBS for 5 min/wash, followed by primary antibody incubation overnight at 4°C in 1% (w/v) BSA/milk and TTBS. A primary antibody against NADP-ME from *Zea mays* was used (courtesy of Robert Sharwood, Western Sydney University, Australia) at 1 : 2000 dilution.

Upon completion of the primary antibody incubation, the membrane was washed four times with TTBS for 5 min per wash. The membrane was then incubated with secondary antibody (HRP conjugated antibody (goat antirabbit IgG (H&L), HRP-conjugated; product no. AS09602, 1 : 10 000 dilution, polyclonal antibody, Agrisera), 1% (w/v) BSA/milk and TTBS) for 1–2 h, followed by washing with TTBS three times and TBS two times at 5 min/wash. Lastly, the membrane was incubated with 7 ml of Clarity Western ECL Substrate (1 : 1 luminol/enhancer solution: peroxide chemiluminescent detection reagent; BIO-RAD Laborotories Inc.) for 5 min before visualization on the transilluminator (G:BOX; Syngene) using the GeneSys software (v.1.7.2; Syngene). Subsequently, Coomassie blue staining (0.05% (w/v) Coomassie brilliant blue G-250, 50% (v/v) methanol, 10% (v/v) glacial acetic acid and adjusted with ultrapure water) was carried out on the same membrane to confirm equal loading. The membrane was incubated with Coomassie blue staining solution for 5 min and stained with the staining solution (40% (v/v) methanol, 10% (v/v) glacial acetic acid), and destaining solution (40% (v/v) methanol, 10% (v/v) with ultrapure water) for 5–10 min. For visualization, the membrane was imaged with a transilluminator (G:BOX; Syngene) using the GeneSys software (v.1.7.2; Syngene, Cambridge, UK).

Enzyme activity assays

Maximum NADP-ME activity was determined following Pengelly *et al.* (2012) and Sharwood *et al.* (2016). Briefly, frozen leaf samples (1.5 cm^2) were homogenized using ice cold mortar and pestle in 900 μl of basic ice-cold extraction buffer containing 50 mM Bicine–NaOH, pH 8.2, 1 mM EDTA, 50 mM 2-mercaptoethanol, 1 mM dithiothreitol, 1% (v/v) protease inhibitor cocktail, and 1% (w/v) polyvinylpyrrolidone in CO_2-sparged deionized H_2O.

The homogenate was centrifuged at 13 000 ***g*** for 1 min, and the supernatant was used in the assay. For each assay, 100 μl of the supernatant was added to 900 μl of the NADP-ME assay buffer (50 mM Bicine–NaOH, pH 8.2, 1 mM EDTA, 5 mM Malate) in a 96-well microtiter plate. The reaction was initiated by adding 10 μl of 200 mM $MgCl_2$. The activity of NADP-ME was calculated by monitoring the decrease in absorbance of NADPH at 340 nm using a diode array spectrophotometer plate reader (Synergy HTX; Agilent Biotek).

Maximal phosphoenol pyruvate carboxylase (PEPC) activity was measured using an NADH-linked assay as described in Sharwood *et al.* (2016). Frozen leaf samples (1.5 cm^2) were homogenized in ice-cold mortar and pestle with 600 μl of extraction buffer (50 mM Bicine–NaOH, pH 8.2, 1 mM EDTA, 50 mM 2-mercaptoethanol, 1 mM dithiothreitol, 1% (v/v) protease inhibitor cocktail, and 1% (w/v) polyvinylpyrrolidone, CO_2-sparged deionized H_2O). The homogenate was centrifuged for 1 min at 13 000 ***g***, and the supernatant was desalted on a Zeba™ spin desalting column (Thermo Scientific). To perform the assay, 5 μl of supernatant was added to 195 μl assay buffer (1 M

© 2026 The Author(s).
New Phytologist © 2026 New Phytologist Foundation.

HEPES-NaOH, pH 8.0, 1 M $MgCl_2$•$6H_2O$, 0.1 M EDTA, 0.5 M $NaHCO_3$, 0.1 M D-glucose 6-phosphate sodium salt, 8.5 KU mL^{-1} malic dehydrogenase (MDH), 14 mM β-nicotinamide adenine dinucleotide (NADH, reduced disodium salt), and 0.2 M phospho(enol)pyruvic acid trisodium salt hydrate) and the reaction was initiated by the addition of 5 µl of 5 mM PEP. The activity was calculated by monitoring the decrease in NADH absorbance at 340 nm with a diode array spectrophotometer plate reader (Synergy HTX; Agilent Biotek, Winooski, VT, USA) after initiating the reaction.

Rubisco initial and total activity were measured from leaf extracts after Sales *et al.* (2020) with slight modifications. Leaf samples (1.5 cm^2) were snap-frozen in liquid nitrogen and stored at −80°C until use. They were then ground in an ice-cold mortar and pestle with 1500 µl of extraction buffer containing 50 mM Bicine–NaOH, pH 8.2, 20 mM $MgCl_2$, 1 mM EDTA, 2 mM benzamidine, 5 mM ε-aminocaproic acid, 50 mM 2-mercaptoethanol, 10 mM dithiothreitol, 1% (v/v) protease inhibitor cocktail (Sigma-Aldrich), and 1 mM phenylmethylsulfonyl fluoride. The homogenate was clarified by centrifugation at 14 000 ***g*** and 4°C for 1 min. The supernatant was immediately used for measuring Rubisco activity at 25°C. For initial activity, the reaction was started by adding 5 µl homogenate to 195 µl complete assay buffer. For total activity, Rubisco in leaf extracts was first activated by incubation in the assay buffer containing CO_2 and Mg^{2+} but in the absence of RuBP for 10 min in the dark, and then the reaction was initiated by adding 6 µl of 20 mM RuBP. The change in absorbance at 340 nm was monitored with a diode array spectrophotometer plate reader (Synergy HTX; Agilent Biotek) after initiating the reactions.

For all enzyme activity assays, measured absorbance values on the microplate plate reader (Synergy HTX; Agilent Biotek) were normalized to a path length of 1 cm (the typical cuvette width used in spectrophotometers (Burnett, 1972)), using a factor of 5.47 mm, considering both the volume and dimensions of the well (Sales *et al.*, 2018). The reaction proceeded for at least 2 min to obtain a clear slope of decreasing absorbance. The first minute of the linear range of the activity was used to calculate the activities.

Gas exchange measurements

All gas exchange measurements were performed using LI-6400XT gas exchange system (LICOR Biosciences, Lincoln, NE, USA) on the youngest fully expanded leaf of 8-wk-old plants. Because blue light and C_i signals are known to converge (Hiyama *et al.*, 2017), we decided to do a complete assessment of stomatal sensitivity to red/blue composition, as well as increasing red light intensity under constant C_i. To characterize stomatal responses to differences in red and blue composition of incident light, leaves were first acclimated under 100% red light for at least 40 min. They were then switched to 75% red (630 nm) and 25% blue light (470 nm) for 60 min, followed by re-exposure to the original light environment of 100% red light for another 60 min. A PPFD of 500 µmol m^{-2} s^{-1} was maintained throughout the experiment. The blue light treatment was initiated when steady state was reached (typically after 2 h). Gas exchange measurements were logged every 60 s throughout the protocol. Reference CO_2 during the experiment was controlled at 400 µmol mol^{-1}, block temperature was kept at 25°C, and average VPD was *c.* 1.2 kPa. All measurements were taken between 10:00 h and 16:00 h.

To further characterize the responses of stomatal conductance to red light intensity while keeping C_i constant, the protocol by Messinger *et al.* (2006) was adopted. This protocol measures the stomatal response to red light while controlling for the potentially confounding effect of the stomatal CO_2 response by maintaining a constant intercellular CO_2 concentration (C_i) at each light intensity. Briefly, the Messinger protocol (Messinger *et al.*, 2006) involved illuminating the leaf segment clamped inside the cuvette with 800 µmol m^{-2} s^{-1} red light to steady state. Subsequently, PFD was lowered stepwise from 800 to 600, 400, 200, 0 µmol m^{-2} s^{-1}. Each change was initiated once steady-state stomatal conductance had been reached, with at least a 40-min waiting period. CO_2 was manually adjusted using the mixer millivolt signal to keep C_i at the value observed at 800 µmol m^{-2} s^{-1}.

Stomatal morphology and density

To estimate stomatal morphology and density, epidermal imprints were taken from adaxial and abaxial layers using clear nail varnish (Rimmel, London, UK) using the same leaves used for gas exchange measurements. Dried nail varnish was lifted from the leaf using sticky tape (Sellotape®; Henkel Ltd, Hemel Hempstead, UK) and affixed onto glass slides. Images were captured using a Nikon microscope (Olympus BX41, Japan) fitted with a CCD camera (U-TV0.5zc-3/Micropublisher 3.3 RTV; Olympus, Tokyo) and installed with Q-Capture Pro 7 imaging software. Total magnifications of ×200 and ×400 (Olympus WHB 10×/20 eyepiece × Olympus PN 20×/0.40 or PCN 60×/0.80 objectives) were used for SD counting and investigation of stomatal anatomical parameters, respectively.

To assess stomatal size (SS), guard cell width, and guard cell length were measured manually using the Fiji software (v.2.14.0; National Institutes of Health, Bethesda, MD, USA). SS was calculated using the formula for the area of an ellipse. SD was calculated as the number of stomata per unit area (mm^2). A stomate was counted if > 50% was located within the field of view. Four random microscopic fields of view each from the adaxial and abaxial surfaces were collected from 3 to 5 biological replicates, giving > 300 stomata per species.

Statistical analyses

To estimate the impact of red and blue light spectral composition on stomatal conductance, a linear mixed-effects model was used. To perform the analysis, g_s and A at specific time points before each switch, and at the end of the R→RB→R experiment (t = 5 min, t = 65 min, and t = 125 min) were extracted from the gas exchange time series. The models included *Genotype* and *Light treatment* (R or RB) as fixed effects, with biological replicate

© 2026 The Author(s).
New Phytologist © 2026 New Phytologist Foundation.

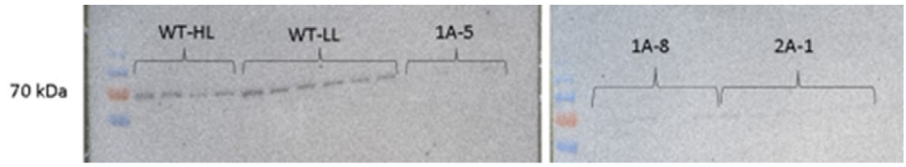


Fig. 1 NADP-malic enzyme (NADP-ME) protein expression in wild-type (WT) plants of *Flaveria bidentis* and plants expressing an antisense construct against NADP-ME. The relative expression level of NADP-ME in WT plants was evaluated when grown under regular light intensity (HL, 350 μmol m^{-2} s^{-1}) and low light intensity (LL, 150 μmol m^{-2} s^{-1}) to match the conditions of the antisense lines. The plants for three independent antisense lines (1A-5, 1A-8, and 2A-1) were grown under the lower intensity to avoid light stress.

(*Replicate*) specified as a random effect to account for repeated measurements.

For the red-light response experiment, a separate linear mixed-effects model was used with *Genotype* and red light photosynthetic PFD (*PPFD*) as fixed effects and *Replicate* as a random effect: *Response variable* ~ *Genotype* x *PFD* + (1|*Replicate*). Model assumptions were verified by inspecting residual distributions and using the Shapiro–Wilk test for normality. Models were fitted using restricted maximum likelihood via the lmer() function from the LME4 (v.1.1-35.5; Bates *et al.*, 2015) package in R (v.4.4.1; R Core Team, 2024). *Post hoc* pairwise comparisons among genotypes were performed on model-estimated means using Tukey's multiplicity adjustment (Tukey–Kramer method) for all pairwise contrasts, implemented though EMMEANS (v.1.10,1; Lenth, 2024) and MULTCOMP (v.1.4-25; Hothorn *et al.*, 2008), with an α level of 0.05.

We used a similar linear mixed-effects model framework to evaluate the effect of genotype on enzyme activities, total soluble protein (TSP), and Chl content. The model included *Genotype* as a fixed effect and biological replication (*Replicate*) as a random effect: *Response variable* ~ *Genotype* + (1|*Replicate*). *Post hoc* pairwise comparisons were performed using Tukey's Honestly Significant Difference (HSD) test at α = 0.05.

The SD on the abaxial and adaxial surfaces was analyzed using a two-way ANOVA, and Tukey's HSD (α = 0.05) was used to separate the means if a significant effect of genotype, leaf side, or their interaction was detected. Data on stomatal size were processed similarly.

Results

NADP-ME activity is decreased by 66–73% in homozygous antisense *Flaveria bidentis* lines

Homozygous transgenic *F. bidentis* T_3 plants with reduced NADP-ME activity via antisense were used for all the presented analyses (see the Materials and Methods section). The effect of the antisense construct on NADP-ME protein content was confirmed by immunoblotting (Fig. 1). Immunolabeling of blotted proteins with an antibody against NADP-ME (provided by Prof Rob Sharwood) showed bands at the predicted size (65 kDa) for WT plants grown under regular (HL) or low light (LL, 150 μmol m^{-2} s^{-1}) (Fig. 1, left panel). By contrast, strongly diminished bands were observed for 1A-5, 1A-8, and 2A-1 plants (Fig. 1), confirming the impact of the antisense construct on NADP-ME protein abundance. To assess the impact of the decrease in NADP-ME protein content, total NADP-ME enzyme activity was assessed using a spectrophotometric assay. Total leaf activity of NADP-ME was significantly reduced ($P < 0.001$) in T_2 homozygous populations of antisense *F. bidentis* plants (Fig. 2a). On average, NADP-ME activity in the antisense lines was 12.4 ± 0.9 μmol m^{-2} s^{-1}, compared to WT, which was 39.3 ± 2.7 μmol m^{-2} s^{-1}, or *c.* 68% reduction in total NADP-ME leaf activity. The reductions in NADP-ME activity in the T_2 antisense lines varied from 66 to 73%, which is less variable than the previously published values in the segregating T_1 populations (Pengelly *et al.* 2012).

Decreasing NADP-ME activity does not significantly affect other key carbon assimilation enzymes

To assess whether the strong reduction NADP-ME activity influenced other key carbon assimilation enzymes, we measured PEPC and Rubisco activities in the same leaves, and extended the analysis to include Chl content and TSP. While genotype significantly affected PEPC activity ($P < 0.0001$), only 1A-5 differed significantly from the WT control; thus, this did not appear to be a common property of NADP-ME downregulation (Fig. 2b). Rubisco activity (Fig. 2c) and Rubisco activation state (Fig. 2d) did not show significant genotype effects ($P = 0.075$ and $P = 0.634$, respectively) and neither did PEPC : Rubisco ratios ($P = 0.680$). Similarly, no significant genotype effects were detected for total Chl content ($P = 0.200$; Fig. 3a) and TSP ($P = 0.842$; Fig. 3b).

Operating intercellular (CO_2) is significantly increased in NADP-ME antisense lines of *F. bidentis*

To find out whether the decrease in NADP-ME activity in antisense lines affected stomatal movements, g_s was assessed both under 100% red light and a mixture of 75% red and 25% blue light (Figs 4a–c, S3). Blue light did not have a significant effect on stomatal opening regardless of genotype. There was also no significant effect of genotype on the overall mean g_s throughout the experiment (mixed model analysis, $P = 0.18$), although the levels in WT plants were slightly lower at 0.125 ± 0.017 mol H_2O m^{-2} s^{-1} than any of the mutants (1A-5 = 0.146 ± 0.011 mol H_2O m^{-2} s^{-1}; 1A-8 = 0.168 ± 0.021 mol H_2O m^{-2} s^{-1}, and 2A-1 = 0.165 ± 0.015 mol H_2O m^{-2} s^{-1}). The analysis of C_i, on the other hand, showed a significant genotype

© 2026 The Author(s).
New Phytologist © 2026 New Phytologist Foundation.

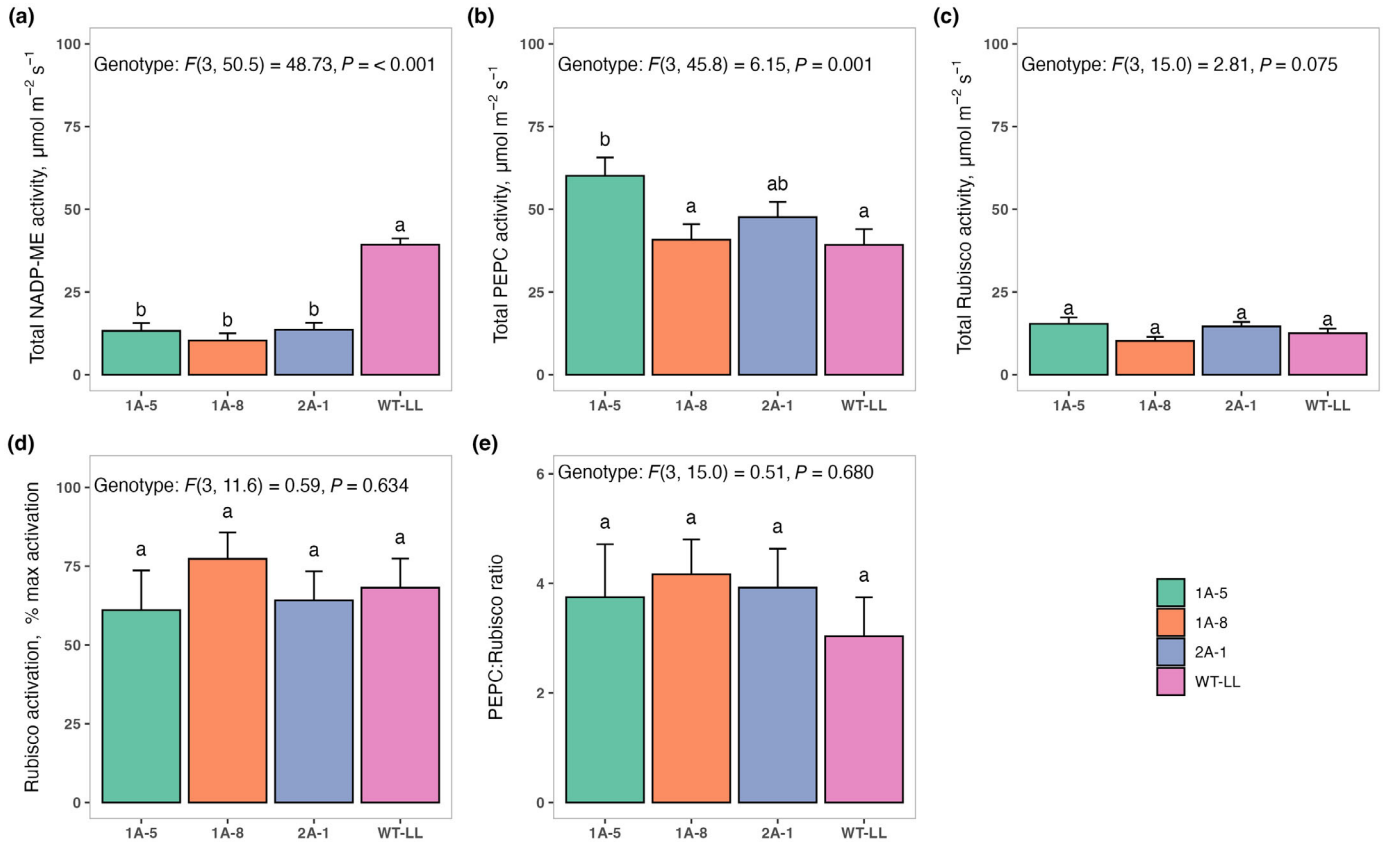


Fig. 2 NADP-malic enzyme (NADP-ME), phosphoenol pyruvate carboxylase (PEPC), and Rubisco activity in wild-type (WT) plants of *Flaveria bidentis* and plants expressing an antisense construct against NADP-ME. Measurements were performed on soluble protein extracted from youngest fully expanded leaves of 8-wk-old plants (n = 3–6). (a) NADP-ME (malic enzyme) activity. (b) PEPC activity (c). Total Rubisco activity (d) Rubisco activation status. (e) PEPC : Rubisco ratio. Values represent the mean ± SE. Statistical analysis was conducted using linear mixed-effects models with genotype as a fixed effect and biological replication as a random effect. Significant differences between genotypes were assessed using model-estimated contrasts based on Tukey's Honestly Significant Difference test. Different letters indicate statistical significance at $\alpha = 0.05$.

effect, with significantly higher values in antisense lines than in the WT control (Fig. 4d–f; $P < 0.05$).

g_s is significantly increased in NADP-ME antisense lines when measured at WT C_i

While g_s under either R or RB light did not vary between the NADP-ME antisense lines and WT control plants, C_i during the measurements was markedly increased in the antisense lines and may have suppressed their level of g_s. Therefore, a follow-up experiment was carried out in which C_i was kept constant at 120 mol CO_2 mol^{-1}, the operating concentration in the WT plants, while incident red light intensity was varied (Fig. 5).

When incident red light intensity was reduced from 800 to 200 µmol photons m^{-2} s^{-1}, the overall g_s for the antisense lines did not change and, ranging from 0.230 ± 0.020 mol H_2O m^{-2} s^{-1} to 0.225 ± 0.014 mol H_2O m^{-2} s^{-1}. WT g_s was also constant across this range of light intensity but showed lower values at 0.151 ± 0.0127 mol H_2O m^{-2} s^{-1} to 0.131 ± 0.0123 mol H_2O m^{-2} s^{-1} (Fig. 5a). As a result, the interaction effect between genotype and light intensity was not significant ($P = 0.9996$), nor was the effect of light intensity ($P = 0.4280$). However, the effect of genotype on g_s was significant ($P < <0.001$), with significantly higher values in the three antisense lines relative to WT ($P < 0.05$).

Not surprisingly, CO_2 assimilation rate responded significantly to the intensity of red light in all genotypes ($P < 0.001$; Fig. 5b). Although the effect of light intensity was highly significant, the interaction between genotype and light level was not ($P = 0.319$), suggesting that antisense and WT plants responded similarly to increasing red light, despite differing baseline assimilation capacities.

Stomatal density and size are altered in NADP-ME antisense lines

To determine whether the g_s differences corresponded to any differences in stomatal patterning or morphology, SD and SS were assessed. As observed previously in WT *F. bidentis* (Bernardo *et al.*, 2023), SD varied between leaf surfaces ($P < 0.0001$) with higher SD and larger stomatal size in the abaxial layer than in the adaxial layer (Fig. 6). SD was slightly reduced in the NADP-ME antisense lines relative to WT, particularly on the adaxial surface, while stomatal size was slightly increased on the abaxial surface in

© 2026 The Author(s).
New Phytologist © 2026 New Phytologist Foundation.

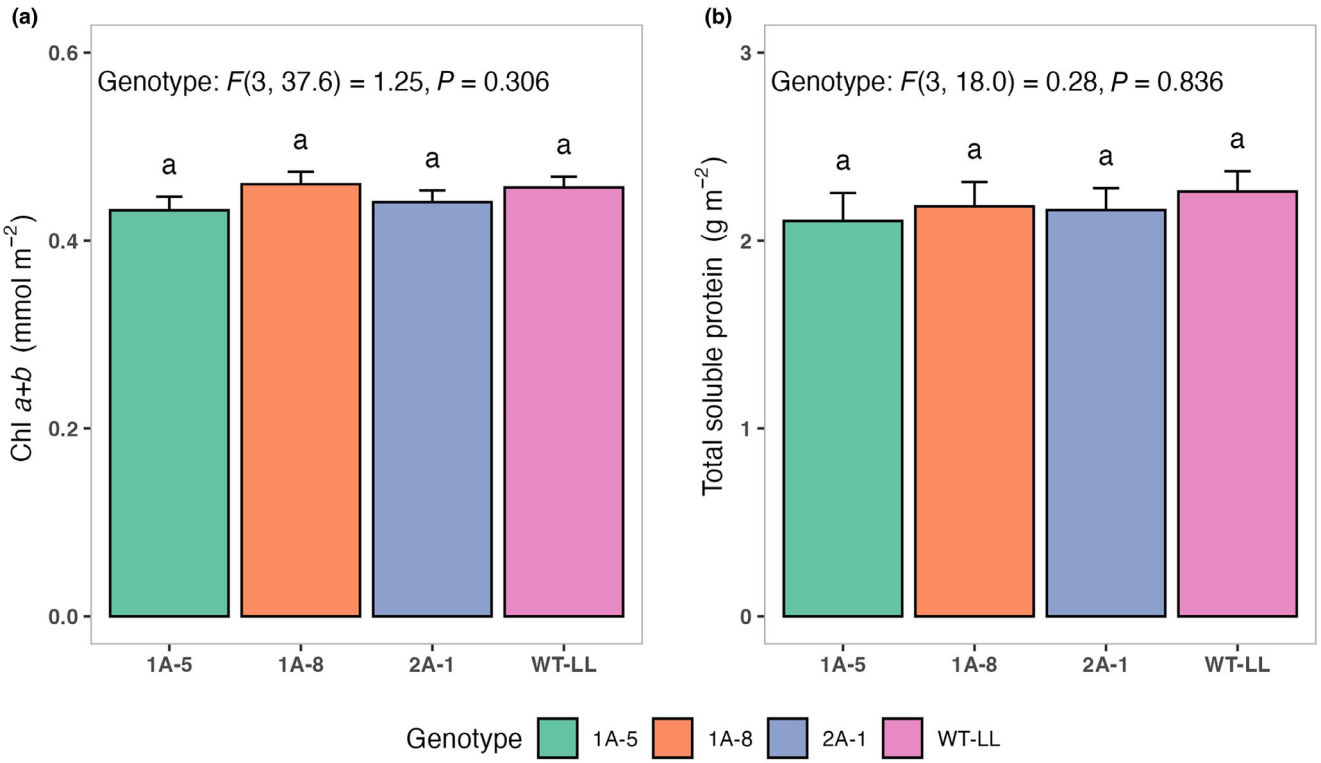


Fig. 3 Chl and total protein content in wild-type (WT) plants of C_4 *Flaveria bidentis* and plants expressing an antisense construct against NADP-malic enzyme. Total Chl (a) and total soluble protein (b) contents were measured spectrophotometrically from crude leaf extracts in 80% EtOH of 8-wk-old plants. Protein content was estimated against Bovine Serum Albumin standards using Bradford assay. Values represent the mean ± SE of n = 4–6. Statistical analysis was conducted using linear mixed-effects models with genotype as a fixed effect and biological replication as a random effect.

two of the antisense lines (1A-5 and 1A-8). Nevertheless, neither of these minor differences seems to be consistent with the observed increase in stomatal conductance, which instead seems to be a consequence of altered CO_2 sensitivity of stomatal aperture changes.

Discussion

This study examined the effect of antisense reduction of NADP-ME activity, the major C_4 acid decarboxylase in the C_4 species *F. bidentis*, on stomatal conductance. Here, perturbation of the C_4 cycle provided a means to investigate coordination between photosynthesis and stomatal conductance in plants with perturbed carbon assimilation while not directly targeting enzymes in the CBB cycle. Antisense suppression of NADP-ME reduced enzyme activity by 66–73% across all lines, yet only moderately decreased light-saturated net CO_2 assimilation (A_n) by 17 to 35%. Despite these significant reductions in A_n, no corresponding decrease in stomatal conductance (g_s) was observed.

Photosynthesis is well-known to affect stomatal apertures by lowering C_i in leaves (Engineer *et al.*, 2016). This has been referred to in literature as the C_i-dependent stomatal red-light response (e.g. Taylor *et al.*, 2024). When the negative impact of decreased photosynthesis on stomatal conductance was removed via assessment at common C_i of WT plants, NADP-ME antisense plants had significantly higher g_s, showing the importance of accounting for effects of the antisense construct on operational C_i when interpreting stomatal responses. In the following paragraphs, we discuss the relevance and wider implications of these findings.

NADP-ME antisense lines lack significant secondary effects

The antisense *F. bidentis* lines with reduced NADP-ME activity used here were originally generated by Pengelly *et al.* (2012), who selected a partially differing subset of independent events for their studies and analyzed the segregating T_1 generation. NADP-ME activities and net assimilation rates of WT control plants found by Pengelly *et al.* (2012) were slightly higher than plants used here, potentially due to the low light intensity required to avoid stress responses in the homozygous antisense plants. The coordination between malate decarboxylation via NADP-ME and RuBP carboxylation via Rubisco in the CBB cycle is critical to maintaining efficient carbon assimilation in C_4 species and avoiding excessive leakiness (Kromdijk *et al.*, 2014). Whereas Pengelly *et al.* (2012) reported slightly enhanced Rubisco and PEPC activity in the NADP-ME antisense plants, this was not observed in this study (Fig. 2c). In addition, Pengelly *et al.* (2012) reported a slight increase in leaf nitrogen content in the antisense plants. Leaf nitrogen content was not evaluated in the present work, but total Chl

© 2026 The Author(s).
New Phytologist © 2026 New Phytologist Foundation.

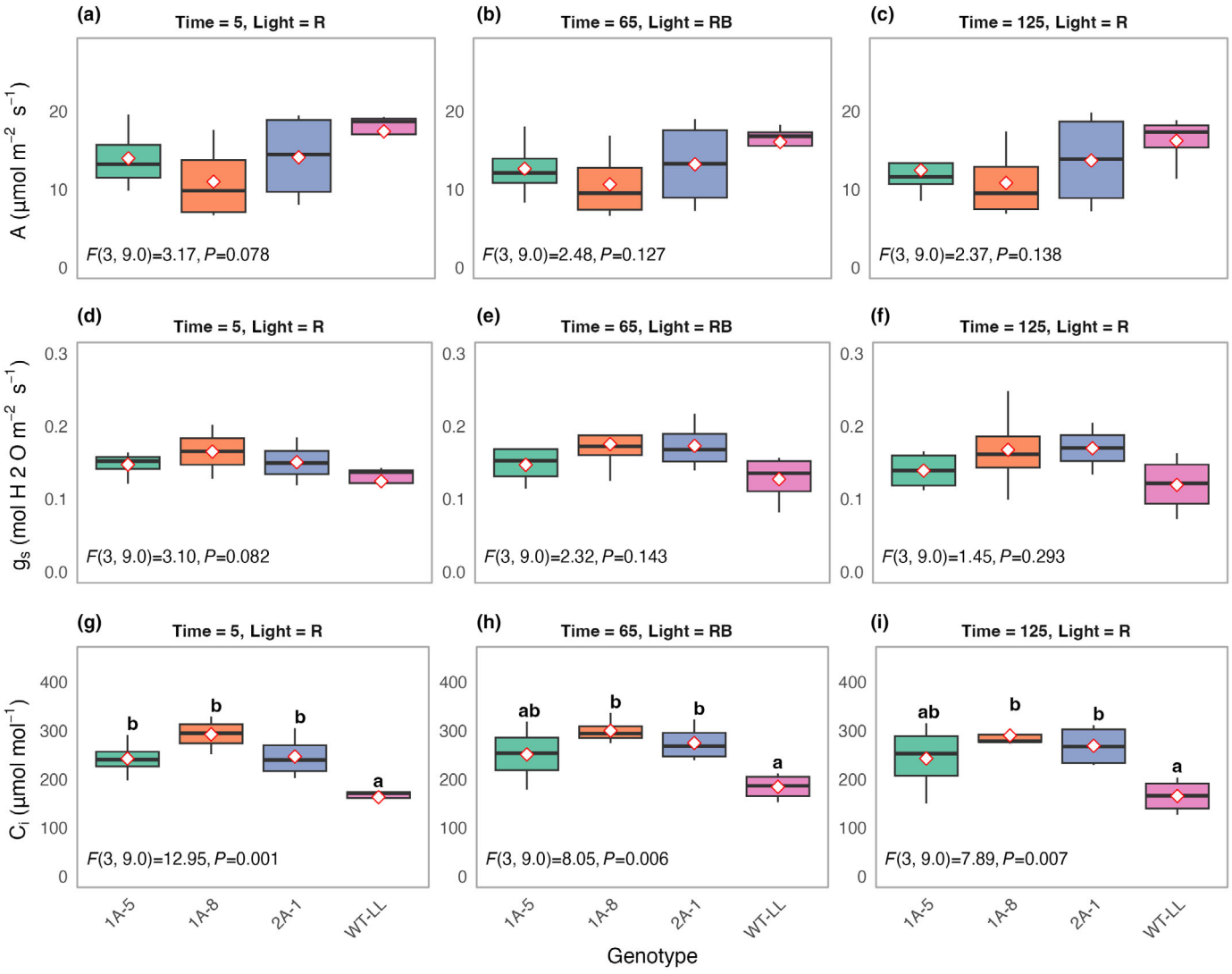


Fig. 4 Stomatal conductance and intercellular CO_2 concentration at two spectral light conditions in wild-type (WT) plants of C_4 *Flaveria bidentis* and plants expressing an antisense construct against NADP-malic enzyme. CO_2 assimilation rate (A; a, b, c), Stomatal conductance (g_s; d, e, f), and intercellular CO_2 concentration (C_i; g, h, i) in WT-LL and three antisense lines of C_4 *F. bidentis* at 5, 65, and 125 mins under specified light conditions. Boxes show interquartile range, horizontal lines show median and whiskers show data range. Full timeseries are provided in Supporting Information Fig. S3. Significant differences in A, g_s, and C*i* were determined using model-estimated means with Tukey's Honestly Significant Difference adjustment at $\alpha = 0.05$. Within each C_i (g–i) time point panel, box plots sharing the same letter are not significantly different. Diamonds indicate group means ($n = 4$).

and protein content were found to be unaffected by the antisense construct (Fig. 3). These slight differences could have resulted from a variety of reasons, including different growing conditions, as well as the use of two different transformation events, and the inclusion of both hemizygous and homozygous plants in the analysis by Pengelly *et al.* (2012). Nevertheless, Pengelly *et al.* (2012) observed decreased CO_2 assimilation and increased C_i/C_a across a range of light intensity, yet similar stomatal conductance in plants with relative NADP-ME reduction similar to the lines analyzed here. While Pengelly *et al.* (2012) did not specifically measure stomatal conductance at common C_i, measurements taken across a range of CO_2 concentrations show that stomatal conductance under the same C_i likely increased in the NADP-ME antisense plants, consistent with our observations.

Evaluating stomatal conductance at common C_i may uncover 'hidden' phenotypes in plants with perturbed photosynthesis rates

Targeting CBB cycle enzymes has been a valuable approach to understand enzyme regulation and the coordination of C_3 and C_4 photosynthetic cycles (Raines, 2003, 2022; Lawson, 2009; Lawson *et al.*, 2010; Lawson & Vialet-Chabrand, 2019). In previous studies on C_3 plants with antisense reductions in Rubisco, decreases of *c.* 35% in Rubisco content caused significant reductions in photosynthesis ranging from 50% in tobacco (Evans *et al.*, 1994) to nearly complete limitation at higher irradiance; yet, these substantial declines in assimilation did not alter stomatal conductance significantly (Hudson *et al.*, 1992; Stitt

© 2026 The Author(s).
New Phytologist © 2026 New Phytologist Foundation.

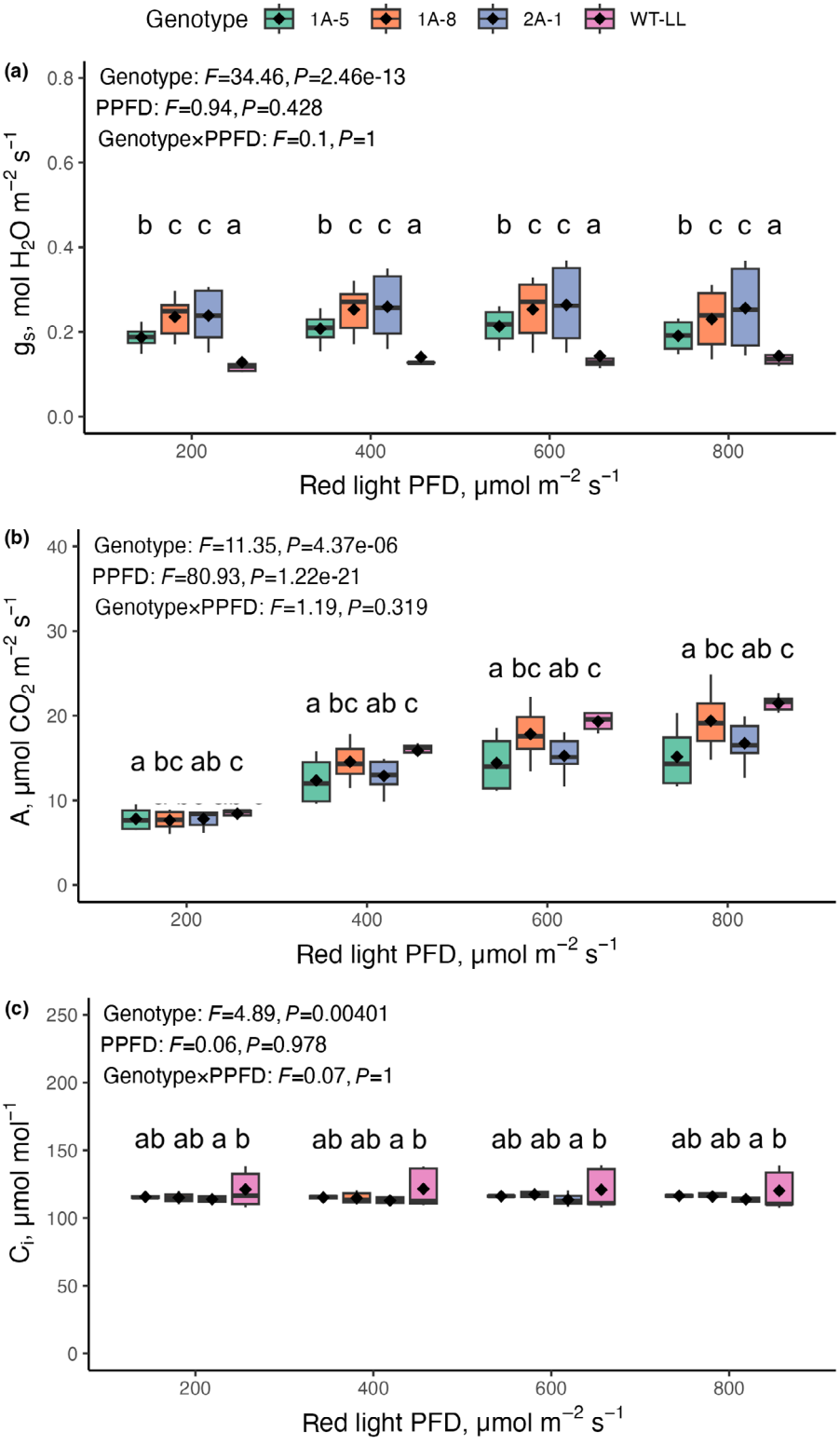


Fig. 5 Stomatal conductance in response to varying light intensity, while keeping C_i constant in wild-type (WT) plants of C_4 *Flaveria bidentis* and plants expressing an antisense construct against NADP-malic enzyme (NADP-ME). Response of stomatal conductance (g_s; a), CO_2 assimilation rate (A_n; b), and intercellular CO_2 concentration (C_i; c) in WT and independent NADP-ME antisense lines of C_4 *F. bidentis* were measured across increasing red light photon flux densities at a common C_i of 120 µmol CO_2 mol^{-1}, matching the WT C_i. Boxes show interquartile range, horizontal lines show median and whiskers show data range. Each box plot represents 4 to 6 biological replicates, with means indicated by black diamonds. Statistical groupings (letters) reflect differences among genotypes as determined by a linear mixed-effects model accounting for replicate effects and evaluated across all light levels.

et al., 1992; Lauerer *et al.*, 1993; Price *et al.*, 1995). Similarly, in antisense *F. bidentis* plants with 34–75% reduction in NADP-ME activity, there was a 30–50% decline in CO_2 assimilation rates in lines with less than 40% NADP-ME activity, particularly at high C_i concentrations; yet, stomatal conductance remained largely unaffected across a range of light intensities and CO_2 levels (Pengelly *et al.*, 2012). Collectively, these studies indicate a surprising lack of stomatal response to considerable reductions in assimilation rates in both C_3 and C_4 systems, highlighting that stomatal regulation can be uncoupled from photosynthetic

© 2026 The Author(s).
New Phytologist © 2026 New Phytologist Foundation.

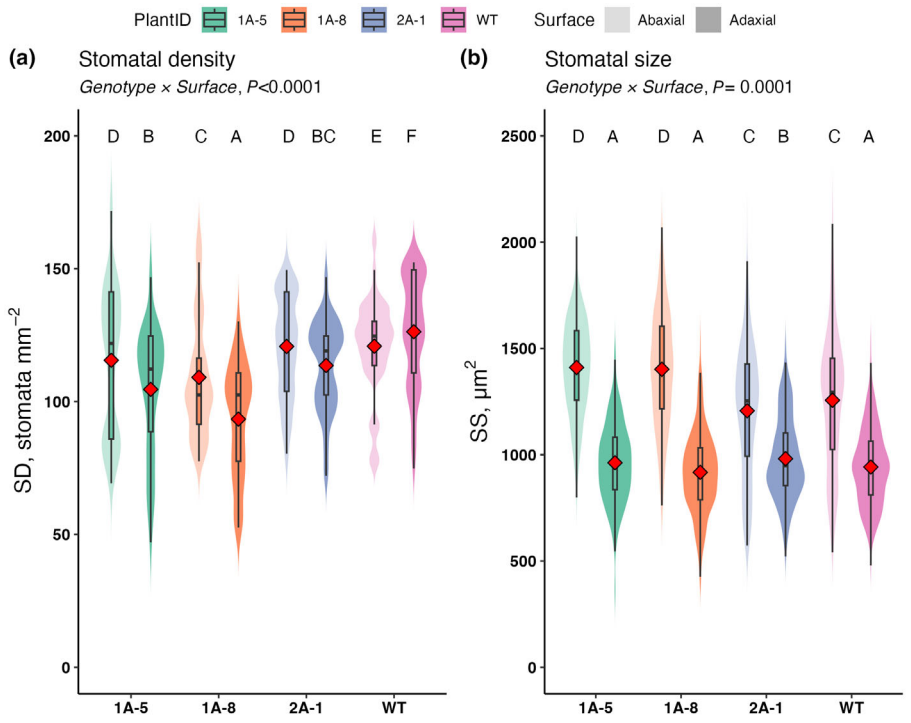


Fig. 6 Stomatal density (SD) and size in wild-type (WT) plants of C_4 *Flaveria bidentis* and plants expressing an antisense construct against NADP-malic enzyme (NADP-ME). SD and size across different mutant lines and WT plants. (a) SD (stomata mm^{-2}) and (b) stomatal size (SS, μm^2) measured on both abaxial and adaxial leaf surfaces in WT and mutant lines (1A-5, 1A-8, 2A-1). For each line, four random microscopic fields of view were collected from both the adaxial and abaxial surfaces of 3–5 independent biological replicates, representing more than 300 individual stomata per genotype. Each violin plot shows the distribution of values per biological replicate, with overlaid boxplots indicating median and interquartile range. Red diamonds represent the mean value for each group. Data were analyzed using a linear mixed model with Genotype, Surface (adaxial vs abaxial), and their interaction (Genotype × Surface) as fixed effects, and biological replicate as a random effect. Estimated marginal means were compared using *emmeans* with a Sidak correction for multiple comparisons ($\alpha = 0.05$). Letters above violin plots indicate groups that are significantly different; groups not sharing a letter are significantly different at $P < 0.05$.

capacity under certain genetic manipulations of photosynthetic enzymes.

When not accounted for, any increases in C_i arising from decreased (or increased) capacity for CO_2 assimilation may lead to dampened (or enhanced) stomatal opening in any transgenic lines with altered photosynthesis. As demonstrated here, when removing the confounding effect of C_i by measuring at a common concentration, a significant increase in stomatal conductance in the antisense plants was uncovered, which was obscured by the opposing C_i effect. It seems plausible that similar effects may manifest more broadly if confounding effects of C_i were accounted for, or at the contrary, observed differences in stomatal conductance under common C_a can be removed under common C_i as demonstrated by observations on SBPase antisense tobacco plants by Lawson *et al.* (2008). The same study also reported a significant C_i-independent component, which is recognized to be part of the stomatal red-light response (Messinger *et al.*, 2006; Matrosova *et al.*, 2015), accounting for *c.* 50% of stomatal red-light responses in *Arabidopsis thaliana* (Taylor *et al.*, 2024). However, in the current work, stomatal responses to changes in red light became negligible in both antisense mutants and WT *F. bidentis* plants when C_i was kept constant, in line with previous observations in WT *F. bidentis* (Bernardo *et al.*, 2023), suggesting that alterations in this response are unlikely to underpin the observed increase in stomatal conductance in the antisense plants.

Keeping C_i constant during gas exchange measurements is relatively trivial but time-consuming, requiring iterative adjustment of C_i via C_a using the instrument CO_2 control settings while counteracting stomatal responses to mitigate the effect of each change in C_a on C_i. However, control of C_i via C_a means that to keep C_i constant, C_a must vary, thus potentially confounding the stomatal response if guard cells are able to sense C_a. The effect of CO_2 on stomatal movements was described as early as Darwin (1898) and Linsbauer (1916), with Heath & Russell (1954) later recognizing the relevance of intercellular CO_2 in this response. Using a split-chamber approach, Mott (1988) demonstrated that stomata exclusively sensed C_i in leaves of two amphistomatous species by showing that stomatal responses to C_i were not affected by varying concentrations in air or at the leaf surface. Since this seminal work, the consensus has been that guard cells exclusively sense C_i. However, the fact that CO_2 sensing is guard cell autonomous (Engineer *et al.*, 2016) and that substantial species variation appears to exist in stomatal sensitivity to CO_2 (Liang *et al.*, 2023), suggests that a contribution of the CO_2 concentration inside the pore in some species may not be ruled out *a*

© 2026 The Author(s).
New Phytologist © 2026 New Phytologist Foundation.

priori, as suggested previously by von Caemmerer *et al.* (2004). Nevertheless, considering the elevated C_i/C_a as a general feature of most transgenic plants with CBB cycle or C_4 cycle impairments, even with a moderate contribution of CO_2 in the pore, the average CO_2 sensed by stomata is likely increased, with the suppressing effect of stomatal opening as a result. Based on this elevation in the concentration sensed by stomata, experiments should also account for potential acclimatory decreases in SD to elevated C_a such as seen in species grown at elevated CO_2 (Hetherington & Woodward, 2003) and across geological timescales with contrasting atmospheric compositions (Woodward, 1987). Alternatively, use of inducible constructs (Schlücking *et al.*, 2013) may allow a more precise way to study the direct impact of mutations on stomatal responses by removing the potentially confounding impact of acclimatory responses to constitutive knockdowns.

The molecular mechanism underlying increased g_s at constant C_i in antisense NADP-ME plants remains unresolved

Our observations in C_4 cycle mutants of *F. bidentis* confirm those of several previous studies on CBB cycle mutants, showing that the negative impacts of decreased CBB cycle or C_4 cycle enzyme expression on CO_2 assimilation are independent of stomatal function *per se*. Indeed, the apparent coordination observed in unperturbed plants does not reflect a direct link between photosynthesis and stomatal conductance, consistent with previous conclusions (for a review, see Lawson *et al.*, 2014). Nevertheless, photosynthesis affects stomatal conductance via its effect on C_i (Lawson, 2009), which should generally lead to a decline in genetic mutant plants with higher C_i. The fact that this is often not observed may imply that the prevailing stomatal conductance in these mutants is not determined by optimization of carbon gain over water loss, but instead reflects stomatal acclimation to the prevailing growth conditions to support alternative functions of transpiration, such as bulk water movement to drive nutrient uptake and translocation (Matimati *et al.*, 2013). While this can be achieved via adjustment of stomatal size and patterning (Casson & Gray, 2008), this was not the case here (Fig. 6). Instead, the fact that stomata in the antisense plants opened more than WT plants under common C_i but not under 'growth C_i' suggests that such acclimation may involve an adjustment of the molecular players involved in sensing and guard cell turgor responses to high C_i. These could include β-CARBONIC ANHYDRASE 1 and 4 (CA1 and CA4), which help to produce bicarbonate that activates S-type anion channels (Xue *et al.*, 2011); the HIGH LEAF TEMPERATURE 1 (HT1) protein kinase (Hashimoto *et al.*, 2006), which suppresses the high CO_2 stomatal closing response by post-translational suppression of OPEN STOMATA 1 (OST1) activity (Horak *et al.*, 2016), which is a positive regulator of the SLOW ANION CHANNEL ASSOCIATED 1 anion channel (Brandt *et al.*, 2012); the RESISTANT TO HIGH CO2 MATE-type transporter, which may act upstream of HT1 to suppress its activity under high CO_2 (Tian *et al.*, 2015), although phenotypes were not consistently repeatable (Toldsepp *et al.*, 2018); and finally, mitogen-activated protein kinases MPK4 and MPK12, which mediate stomatal CO_2 responses (Toldsepp *et al.*, 2018) via inhibition of HT1 activity (Horak *et al.*, 2016). It seems plausible that small acclimatory adjustments in expression or post-translational modification could give rise to the observed phenotypes.

An alternative hypothesis could be that guard cell malate pools are affected by the antisense construct. Malate is involved in stomatal opening as a counterion for potassium accumulation to keep membrane potential by balancing charge (Allaway, 1973; Outlaw Jr & Lowry, 1977). Work by Cousins *et al.* (2007) on the C_4 species *Amaranthus edulis* showed that strong antisense reduction of PEPC to 3% of WT levels led to slower stomatal opening and lower steady state conductance, which was suggested to stem from slower and less abundant malate formation in guard cells. Based on recent single nucleus and single-cell RNAseq data on *F. bidentis* (Sun *et al.*, 2025), it is clear that while the antisense construct was raised against the C_4 NADP-ME isoform (FBID-00003378; Fig. S4A), there is 89.9% sequence conservation of the antisense fragment with the main chloroplastic isoform expressed in guard cells (F-bidentis-14-000158; Fig. S4B). It is therefore plausible that the antisense construct against NADP-ME used in the present work also decreased NADP-ME activity in the guard cells. If so, the resulting alteration in guard cell malate metabolism may have affected g_s in the opposite way compared to the PEPC antisense observations by Cousins *et al.* (2007). During stomatal closure, malate is decarboxylated to pyruvate by NADP-ME, which is then completely oxidized in the mitochondrial tricarboxylic acid cycle. Alternatively, malate can be converted to PEP via the combined action of NAD^+-dependent MDH and PEP carboxykinase (PEPCK) (Santelia & Lawson, 2016). Thus, if NADP-ME activity in guard cells decreased in antisense lines, accumulated malate during stomatal opening may not be as rapidly metabolized, which could give rise to increased stomatal opening and slower stomatal closure, in line with the observed higher g_s at common C_i.

Conclusion

This study focused on the consequences of a disrupted C_4 cycle on the regulation of g_s. The results showed that at common C_a, NADP-ME antisense lines of C_4 *F. bidentis* had similar stomatal conductance but a higher operational C_i than WT, whereas measurements at a common C_i showed an increase in g_s in the antisense lines. These findings are most consistent with altered guard cell C_i sensitivity in the antisense lines. We postulate that altered CO_2 sensing in guard cells may provide a molecular explanation for the increase in g_s in common C_i.

Acknowledgements

This study was supported by a scholarship awarded to ELB through the Foreign Graduate Scholarship Program of the Department of Science and Technology – Science Education Institute (DOST-SEI, Philippines) and new lecturer start-up funding by the Gatsby Foundation to JK. We thank Dr Susanne

© 2026 The Author(s).
New Phytologist © 2026 New Phytologist Foundation.

von Caemmerer for providing seeds of the *F. bidentis* antisense lines, and Prof. Robert Sharwood (Western Sydney University, Australia) for the primary antibody against NADP-ME. We are also grateful to the Department of Plant Sciences and Emmanuel College, University of Cambridge, for the bursary awarded to ELB. Special thanks to Dr Julia Walter (Department of Plant Sciences, University of Cambridge) for her assistance with copy number analysis, SDS-PAGE, and immunoblotting.

Competing interests

None declared.

Author contributions

JK conceptualized the study. ELB managed plant growth and maintenance, performed preliminary testing on wild-type and mutant plants, conducted gas exchange experiments and collected, processed and analyzed the data. ELB and CRS carried out the enzyme activity assays and Chl content determination. TS provided cell-specific expression data for NADP-ME isoforms. ELB and JK drafted the initial manuscript. All authors reviewed and approved the final manuscript.

ORCID

Emmanuel L. Bernardo https://orcid.org/0000-0003-3263-6639
Johannes Kromdijk https://orcid.org/0000-0003-4423-4100
Cristina Rodrigues Gabriel Sales https://orcid.org/0000-0002-8748-7370
Tianshu Sun https://orcid.org/0000-0003-2309-5666

Data availability

All data that support the findings of this study are available in the main text and Figs S1–S4 of this article.

References

Allaway W. 1973. Accumulation of malate in guard cells of *Vicia faba* during stomatal opening. *Planta* **110**: 63–70.

Bates D, Mächler M, Bolker B, Walker S. 2015. Fitting linear mixed-effects models using lme4. *Journal of Statistical Software* **67**: 1–48.

Bernardo EL, Sales CRG, Cubas LA, Vath RL, Kromdijk J. 2023. A comparison of stomatal conductance responses to blue and red light between C_3 and C_4 photosynthetic species in three phylogenetically-controlled experiments. *Frontiers in Plant Science* **14**: 125397.

Brandt B, Brodsky DE, Xue S, Negi J, Kangasjarvi J, Ghassemian M, Stephan AB, Hu H, Schroeder JI. 2012. Reconstitution of abscisic acid activation of SLAC1 anion channel by CPK6 and OST1 kinases and branched ABI1 PP2C phosphatase action. *PNAS* **109**: 10593–10598.

Burnett RW. 1972. Accurate measurement of molar absorptivities. *Journal of Researchof the National Bureau of Standards. Section A, Physics and Chemistry* **76**: 483.

von Caemmerer S, Lawson T, Oxborough K, Baker NR, Andrews TJ, Raines CA. 2004. Stomatal conductance does not correlate with photosynthetic capacity in transgenic tobacco with reduced amounts of Rubisco. *Journal of Experimental Botany* **55**: 1157–1166.

Casson S, Gray JE. 2008. Influence of environmental factors on stomatal development. *New Phytologist* **178**: 9–23.

Cousins AB, Baroli I, Badger MR, Ivakov A, Lea PJ, Leegood RC, von Caemmerer S. 2007. The role of phospho enol pyruvate carboxylase during C_4 photosynthetic isotope exchange and stomatal conductance. *Plant Physiology* **145**: 1006–1017.

Darwin F. 1898. Observations on stomata [Abstract]. *Proceedings of the Royal Society of London* **63**: 413–417.

Engineer CB, Hashimoto-Sugimoto M, Negi J, Israelsson-Nordström M, Azoulay- Shemer T, Rappel WJ, Iba K, Schroeder JI. 2016. CO_2 sensing and CO_2 regulation of stomatal conductance: advances and open questions. *Trends in Plant Science* **21**: 16–30.

Evans JR, Caemmerer S, Setchell BA, Hudson GS. 1994. The relationship between CO_2 transfer conductance and leaf anatomy in transgenic tobacco with a reduced content of rubisco. *Functional Plant Biology* **21**: 475–495.

Farquhar GD, Sharkey TD. 1982. Stomatal conductance and photosynthesis. *Annual Review of Plant Physiology* **33**: 317–345.

Fitzsimons PJ, Weyers JD. 1986. Volume changes of *Commelina communis* guard cell protoplasts in response to K^+, light and CO_2. *Physiologia Plantarum* **66**: 463–468.

Fricker M, Willmer C. 2012. *Stomata.* Dordrecht, the Netherlands: Springer Science & Business Media.

Furbank RT, Chitty JA, von Caemmerer S, Jenkins CL. 1996. Antisense RNA inhibition of RbcS gene expression reduces Rubisco level and photosynthesis in the C_4 plant *Flaveria bidentis*. *Plant Physiology* **111**: 725–734.

Glowacka K, Kromdijk J, Leonelli L, Niyogi KK, Clemente TE, Long SP. 2016. An evaluation of new and established methods to determine T-DNA copy number and homozygosity in transgenic plants. *Plant, Cell & Environment* **39**: 908–917.

Hashimoto M, Negi J, Young J, Israelsson M, Schroeder JI, Iba K. 2006. *Arabidopsis* HT1 kinase controls stomatal movements in response to CO_2. *Nature Cell Biology* **8**: 391–397.

Heath OVS, Russell J. 1954. Studies in stomatal behaviour. VI. An investigation of the light response of wheat stomata with the attempted elimination of control by the Mesophyll. Part II. *Journal of Experimental Botany* **5**: 269–292.

Hetherington AM, Woodward FI. 2003. The role of stomata in sensing and driving environmental change. *Nature* **424**: 901–908.

Hiyama A, Takemiya A, Munemasa S, Okuma E, Sugiyama N, Tada Y, Murata Y, Shimazaki K. 2017. Blue light and CO2 signals converge to regulate light-induced stomatal opening. *Nature Communications* **8**: 1284.

Horak H, Sierla M, Toldsepp K, Wang C, Wang YS, Nuhkat M, Valk E, Pechter P, Merilo E, Salojärvi J *et al.* 2016. A dominant mutation in the HT1 kinase uncovrs roles of MAP kinases and GHR1 in CO_2 induced stomatal closure. *Plant Cell* **28**: 2493–2509.

Hothorn T, Bretz F, Westfall P. 2008. Simultaneous inference in general parametric models. *Biometrical Journal* **50**: 346–363.

Hudson GS, Evans JR, von Caemmerer S, Arvidsson YB, Andrews TJ. 1992. Reduction of ribulose-1,5-bisphosphate carboxylase/oxygenase content by antisense RNA reduces photosynthesis in transgenic tobacco plants. *Plant Physiology* **98**: 294–302.

Kromdijk J, Ubierna N, Cousins AB, Griffiths H. 2014. Bundle-sheath leakiness in C4 photosynthesis: a careful balancing act between CO_2 concentration and assimilation. *Journal of Experimental Botany* **65**: 3443–3457.

Lauerer M, Saftic D, Quick W, Labate C, Fichtner K, Schulze E-D, Rodermel S, Bogorad L, Stitt M. 1993. Decreased ribulose-1,5-bisphosphate carboxylase-oxygenase in transgenic tobacco transformed with "antisense" rbcS: Vi. Effect on photosynthesis in plants grown at different irradiance. *Planta* **190**: 332–345.

Lawson T. 2009. Guard cell photosynthesis and stomatal function. *New Phytologist* **181**: 13–34.

Lawson T, Lefebvre S, Baker NR, Morison JI, Raines CA. 2008. Reductions in mesophyll and guard cell photosynthesis impact on the control of stomatal responses to light and CO_2. *Journal of Experimental Botany* **59**: 3609–3619.

Lawson T, Simkin AJ, Kelly G, Granot D. 2014. Mesophyll photosynthesis and guard cell metabolism impacts on stomatal behaviour. *New Phytologist* **203**: 1064–1081.

Lawson T, Vialet-Chabrand S. 2019. Speedy stomata, photosynthesis and plant water use efficiency. *New Phytologist* **221**: 93–98.

© 2026 The Author(s).
New Phytologist © 2026 New Phytologist Foundation.

Lawson T, von Caemmerer S, Baroli I. 2010. Photosynthesis and stomatal behaviour. *Progress in Botany* **72**: 265–304.

Lenth RV. 2024. *EMMEANS: estimated marginal means, aka least-squares means. R package v.11.* [WWW document] URL https://rvlenth.github.io/emmeans/.

Liang X, Wang D, Ye Q, Zhang J, Liu M, Liu H, Yu K, Wang Y, Hou E, Zhong B *et al.* 2023. Stomatal responses of terrestrial plants to global change. *Nature Communications* **14**: 2188.

Linsbauer K. 1916. Beitrage zur kenntnis der spaltoffnungsbewegungen. *Flora* **9**: 100–143.

Marshall JS, Stubbs JD, Taylor WC. 1996. Two genes encode highly similar chloroplastic NADP-malic enzymes in *Flaveria* (implications for the evolution of C_4 photosynthesis). *Plant Physiology* **111**: 1251–1261.

Matimati I, Verboom GA, Cramer MD. 2013. Nitrogen regulation of transpiration controls mass-flow acquisition of nutrients. *Journal of Experimental Botany* **65**: 159–168.

Matrosova A, Bogireddi H, Mateo-Peñas A, Hashimoto-Sugimoto M, Iba K, Schroeder JI, Israelsson-Nordström M. 2015. The ht1 protein kinase is essential for red light-induced stomatal opening and genetically interacts with ost1 in red light and CO_2-induced stomatal movement responses. *New Phytologist* **208**: 1126–1137.

Messinger SM, Buckley TN, Mott KA. 2006. Evidence for involvement of photosynthetic processes in the stomatal response to CO_2. *Plant Physiology* **140**: 771–778.

Mott KA. 1988. Do stomata respond to CO_2 concentrations other than intercellular? *Plant Physiology* **86**: 200–203.

Mott KA. 2009. Opinion: stomatal responses to light and CO_2 depend on the mesophyll. *Plant, Cell & Environment* **32**: 1479–1486.

Muschak M, Willmitzer L, Fisahn J. 1999. Gas-exchange analysis of chloroplastic fructose-1,6-bisphosphatase antisense potatoes at different air humidities and at elevated CO_2. *Planta* **209**: 104–111.

Outlaw WH Jr, Lowry OH. 1977. Organic acid and potassium accumulation in guard cells during stomatal opening. *Proceedings of the National Academy of Sciences, USA* **74**: 4434–4438.

Paul MJ, Knight JS, Habash D, Parry MAJ, Lawlor DW. 1995. Reduction in phosphoribulokinase activity by antisense RNA in transgenic tobacco: effect on CO_2 assimilation and growth in low irradiance. *The Plant Journal* **7**: 535–542.

Pengelly JJ, Sirault XR, Tazoe Y, Evans JR, Furbank RT, Von Caemmerer S. 2010. Growth of the C4 dicot *Flaveria bidentis*: photosynthetic acclimation to lowlight through shifts in leaf anatomy and biochemistry. *Journal of Experimental Botany* **6**: 4109–4122.

Pengelly JJ, Tan J, Furbank RT, von Caemmerer S. 2012. Anti-sense reduction of NADP-malic enzyme in *Flaveria bidentis* reduces flow of CO_2 through the C_4 cycle. *Plant Physiology* **160**: 1070–1080.

Pignon CP, Long SP. 2020. Retrospective analysis of biochemical limitations to photosynthesis in 49 species: C_4 crops appear still adapted to preindustrial atmospheric [CO2]. *Plant, Cell & Environment* **43**: 2606–2622.

Price GD, Evans JR, von Caemmerer S, Yu J-W, Lloyd J, Oja V, Kell P, Ghannoum O, Boag S, Badger MR. 1995. Specific reduction of chloroplast glyceraldehyde-3-phosphate dehydrogenase activity by antisense RNA reduces CO_2 assimilation via a reduction in ribulose bisphosphate regeneration in transgenic tobacco plants. *Planta* **195**: 369–378.

R Core Team. 2024. *R: a language and environment for statistical computing.* Vienna, Austria: R Foundation for Statistical Computing.

Raines CA. 2003. The Calvin cycle revisited. *Photosynthesis Research* **75**: 1–10.

Raines CA. 2022. Improving plant productivity by re-tuning the regeneration of RuBP in the Calvin-Benson-Bassham cycle. *New Phytologist* **236**: 350–356.

Sales CR, da Silva AB, Carmo-Silva E. 2020. Measuring Rubisco activity: challenges and opportunities of NADH-linked microtiter plate-based and ^{14}C-based assays. *Journal of Experimental Botany* **71**: 5302–5312.

Sales CR, Degen GE, da Silva AB, Carmo-Silva E. 2018. Spectrophotometric determination of Rubisco activity and activation state in leaf extracts. *Photosynthesis: Methods and Protocols* **177**: 239–250.

Santelia D, Lawson T. 2016. Rethinking guard cell metabolism. *Plant Physiology* **172**: 1371–1392.

Schlücking K, Edel KH, Köster P, Drerup MM, Eckert C, Steinhorst L, Waadt R, Batistic O, Kudla K. 2013. A new β-estradiol-inducible vector set that facilitates easy construction and efficient expression of transgenes reveals CBL3-dependent cytoplasm to tonoplast translocation of CIPK5. *Molecular Plant* **6**: 1814–1829.

Sharwood RE, Ghannoum O, Whitney SM. 2016. Prospects for improving CO_2 assimilation in C_3 crops through understanding C_4-Rubisco biogenesis and catalytic diversity. *Current Opinion in Plant Biology* **31**: 135–142.

Stitt M, Quick W, Schurr U, Schulze E-D, Rodermel S, Bogorad L. 1992. Decreased ribulose-1,5-bisphosphate carboxylase-oxygenase in transgenic tobacco transformed with "antisense" *rbcS*. *Planta* **188**: 522–531.

Sun T, Bonthala VS, Stich B, Luginbuehl LH, Hibberd JM. 2025. Conserved spatial patterning of gene expression in independent lineages of C_4 plants. *New Phytologist* **249**: 24–38.

Taylor G, Walter J, Kromdijk J. 2024. Illuminating stomatal responses to red light: establishing the role of C_i-dependent versus -independent mechanisms in control of stomatal behaviour. *Journal of Experimental Botany* **75**: 6810–6822.

Taylor G, Walter J, Kromdijk J. 2025. Chloroplast-derived hydrogen peroxide coordinates photosynthesis with stomatal opening. *bioRxiv* doi: 10.1101/2025.03.27.645763.

Tian W, Hou C, Ren Z, Pan Y, Jia J, Zhang H, Bai F, Zhang P, Zhu H, He Y *et al.* 2015. A molecular pathway for CO_2 response in *Arabidopsis* guard cells. *Nature Communications* **6**: 6057.

Toldsepp K, Zhang J, Takahashi Y, Sindarovska Y, Horak H, Ceciliato PHO, Koolmeister K, Wang Y-S, Vaahtera L, Jakobson L *et al.* 2018. Mitogen-activated protein kinases MPK4 and MPK12 are key components mediating CO_2-induced stomatal movements. *The Plant Journal* **96**: 1018–1035.

Torii KU. 2015. Stomatal differentiation: the beginning and the end. *Current Opinion in Plant Biology* **28**: 16–22.

Wintermans JFGM, De Mots A. 1965. Spectrophotometric characteristics of chlorophylls a and b and their pheophytins in ethanol. *Biochimica et Biophysica Acta (BBA) - Biophysics including Photosynthesis* **109**: 448–453.

Woodward FI. 1987. Stomatal numbers are sensitive to increases in CO_2 from preindustrial levels. *Nature* **327**: 617–618.

Xue S, Hu H, Ries A, Merilo E, Kollist H, Schroeder JI. 2011. Central functions of bicarbonate in S-type anion channel activation and OST1 protein kinase in CO2 signal transduction in guard cell. *EMBO Journal* **30**: 1645–1658.

Supporting Information

Additional Supporting Information may be found online in the Supporting Information section at the end of the article.

Fig. S1 Bleaching of antisense NADP-ME plants under 350 μmol m^{-2} s^{-1} light intensity is mitigated by 150 μmol m^{-2} s^{-1} light intensity.

Fig. S2 Representative image of wild-type *Flaveria bidentis* plants and three lines carrying independent insertions of the NADP-ME antisense construct.

Fig. S3 Time course of g_s in WT and NADP-ME antisense lines of C_4 *Flaveria bidentis*.

Fig. S4 Expression of different NADP-ME isoforms across contrasting cell types.

Please note: Wiley is not responsible for the content or functionality of any Supporting Information supplied by the authors. Any queries (other than missing material) should be directed to the *New Phytologist* Central Office.

Disclaimer: The New Phytologist Foundation remains neutral with regard to jurisdictional claims in maps and in any institutional affiliations.

© 2026 The Author(s).
New Phytologist © 2026 New Phytologist Foundation.